

DETERMINING MATERIAL TYPE AND TOOL WEAR IN UNDERGROUND MINING VIA
CAPACITIVE LOAD CELLS AND ACOUSTIC SPECTRA ANALYSIS, DESIGN AND
CHARACTERIZATION OF A SMART BIT FOR IN-SITU FORCE MEASUREMENT.

by

Austin F. Oltmanns

© Copyright by Austin F. Oltmanns, 2024

All Rights Reserved

A thesis submitted to the Faculty and the Board of Trustees of the Colorado School of Mines in partial fulfillment of the requirements for the degree of Doctor of Philosophy (Robotics).

Golden, Colorado

Date _____

Signed: _____

Austin F. Oltmanns

Signed: _____

Dr. Andrew J. Petruska
Thesis Advisor

Signed: _____

Dr. Secondary B. Advisor
Thesis Advisor

Golden, Colorado

Date _____

Signed: _____

Dr. Big Boss
Department Head Title
Department of Mechanical Engineering

ABSTRACT

Underground coal miners continue to be exposed to hazards on a routine basis. The best way to mitigate this is removing the operator from the hazardous locations while increasing overall productivity. This work investigates methods for determining tool wear and material type with a sensing system, which would enable operators to make decisions using objective feedback from a safer location. Machine operators must determine tool wear and material type during operation, and when they get close to the cutting interface, they place themselves at risk. Vibration frequencies, acoustic emissions, and cutting forces are all shown to vary with the tested cutting conditions. Three different sensor designs were tested and used: a dynamic capacitive load cell to classify material type and tool wear conditions, an acoustic sensor that does that same, and a capacitive load cell which measures the cutting forces and works with a linear model. The capacitive load cell, when used with a small neural network regression and a 2nd order polynomial expansion, is able to measure rock cutting forces with a mean absolute error less than 4 kilonewtons and an R^2 score greater than 0.8 under tested conditions. Performing material and tool wear classification is done with machine learning classification methods. The Support-Vector machine using fast Fourier spectra magnitude of short samples of signal, around 0.2 seconds, performed the best. Rock cutting tests are performed using a linear cutting machine at the Earth Mechanics Institute on campus. Analytical models for the capacitive sensors are developed as part of this research, and they can be used to guide future designs. This work discusses the sensitivity to input force of the designed sensors. These models also guide the choice of classification methods used to determine material type and tool wear, which are shown to perform well for the experimental conditions.

TABLE OF CONTENTS

ABSTRACT	iii
LIST OF FIGURES	vi
LIST OF TABLES	viii
LIST OF SYMBOLS	ix
LIST OF ABBREVIATIONS	x
ACKNOWLEDGMENTS	xi
DEDICATION	xii
CHAPTER 1 INTRODUCTION	1
CHAPTER 2 MINING SAFETY BACKGROUND	3
CHAPTER 3 SENSORS TECHNOLOGY LITERATURE REVIEW	4
CHAPTER 4 CLASSIFICATION AND REGRESSION TECHNIQUES	5
CHAPTER 5 CAPACITIVE LOAD CELLS TO PROMOTE WORKER SAFETY	6
5.1 Abstract	6
5.2 Introduction	6
5.3 Material and Wear Classification	9
5.3.1 Classification Methods	10
5.3.2 Sensor Design Literature Review	14
5.3.3 Sensor Design	15
5.3.4 Sensor Characterization	17
5.4 Rock Cutting Experiment	17
5.5 Classification Results	19
5.6 Discussion	21
5.7 Conclusion	25
5.8 Disclosures	25
5.8.1 Conflicts of interests	25

CHAPTER 6 YOUR JOURNAL PAPER TITLE GOES HERE	26
6.1 Abstract	26
6.2 Introduction	26
6.3 Permissions	26
6.4 The next section of the paper	26
CHAPTER 7 THIS IS THE TITLE OF A PAPER INCLUDED IN A THESIS	28
7.1 Abstract	28
7.2 Introduction	28
CHAPTER 8 LOAD CELL DESIGN COMPARISON	29
CHAPTER 9 LONGER DOWNSAMPLING RATES FOR ACOUSTIC CLASSIFICATION	30
CHAPTER 10 ANALYTICAL MODEL FITTING	31
REFERENCES	32
SELECTED BIBLIOGRAPHY	37
APPENDIX SPECIAL COOLNESS.	38

LIST OF FIGURES

Figure 1.1	Continous Miner. Pictured is the ‘Remote Continuous Miner HM21 Joy Used for underground coal mining’, originally uploaded to Wikipedia by user Xlxgoggaxlx under the Creative Commons Attribution-Share Alike 3.0 Unported license The machine operator must stand close to the machine and cutting interface to control the machine. The operators use many cues, but ultimately must track if they are cutting the target material and the state of tool wear. Allowing operators to maintain a greater distance while giving them the feedback they require can improve production and safety. Image Source/License: https://commons.wikimedia.org/wiki/File:Continuous_Miner.jpg	1
Figure 5.1	A prototype of the sensor integrated with the U92 4.0 22NB Conical Pick and K35 Block system, from Kennametal. The device is shown without the measurement collection system and is situated between the sleeve and the block. The FlexPCB interface is exposed, which provides access to the capacitive sensors’ electrodes. A steel case protects the FlexPCB sensor and provides the necessary stiffness to transfer the input forces to the sensor. An embedded electronics platform, not shown in this figure, takes measurements suitable for dynamic classification of tool-wear and material. A cutaway of the sensor shows the thin film design for the force sensor.	8
Figure 5.2	The different pick wear levels. The <i>new</i> , <i>moderate</i> , and <i>worn</i> pick tips have spherical diameters of 3.71 mm, 17.9 mm, and 27.5 mm respectively. This approximates and even wear pattern. The <i>moderate</i> and <i>worn</i> tips were artificially worn using a lathe. . . .	8
Figure 5.3	A cutaway of the sensor with the geometric parameters shown. The dimensions of the walls may be tuned to give the sensor the appropriate stiffness. The thickness of the top and bottom plates do not significantly influence the overall stiffness of the device. . . .	16
Figure 5.4	The triangular load profiles and the resulting measurements from the sensor. The sensor response is not symmetric and therefore non-linear. Lower load rates cause greater changes in displacement, which is consistent with previous studies for thin film polyimide.	17
Figure 5.5	The case deformation during the load frame tests. The case deformation is symmetric for the loading and unloading phases, it also has a consistent slope for force over displacement. This means the case has approximately linear deformation for these load profiles.	18
Figure 5.6	The Linear Cutting Machine in action. Hydraulic actuators push the sample into the cutting tool while the custom sensor and the embedded strain gauges record measurements. The tool is normally surrounded by the plastic curtain to aid in capturing dust for a simultaneous study of the effect of tool wear on dust generation. . . .	19
Figure 5.7	Measurements for typical rock cuts with different tool wear levels. The measurements from the linear sensors are shown in the top graph while the measurements from the custom sensor are shown below.	21

Figure 5.8	The frequency signature distributions collected from the custom sensor organized by material. The concrete material shows exponential decay after each primary mode, while the limestone has a more varied response. These differences can be used for classification of the signals by material.	22
Figure 5.9	The frequency signature distributions collected from the custom sensor organized by tool wear. The New tool has a distinct response compared to the Moderate and Worn tools, and the energy in the higher modes generally increases with wear. These differences can be used for classification of the signals by tool wear.	23
Figure 5.10	Bar chart with error bars for F1 score distributions by window size. For tool wear, both sensors were able to provide sufficient data for very accurate classification. For material classification, the capacitive sensor generally performed better than the strain gauge sensor. Some of the differences in performance are significant within the application and sensor combinations, but in general performance was similar across window sizes.	24
Figure 5.11	Performance of different preprocessing methods for each application. In general, normalization after transformation proved most effective for the frequency based techniques. Using the normalized time domain data was most effective for tool wear classification.	24

LIST OF TABLES

Table 5.1	Preprocessing Pipeline Steps, $\ \cdot\ $, \cdot^2 , and $\sqrt{\cdot}$ are element-wise absolute value, square, and square root respectively.	12
Table 5.2	Scoring metric and test/train ratios for each application	20
Table 5.3	Confusion Matrix for Material Classifier; Normalized by prediction New Picks, 0.3 in Penetration, 0.2s Window, 50:50 test and train, PSD w/ post norm.	21
Table 5.4	Confusion Matrix for Tool Wear Classifier; Normalized by prediction All Materials, All Penetrations, 0.2s Window, 50:50 test and train, Normalized Time Domain Data	25

LIST OF SYMBOLS

Average radius of cylindrical shell c

activation energy of oxidation reaction of a-C in excited state E_{act}^*

General Nomenclature

absorption cross section α_σ

LIST OF ABBREVIATIONS

Bio Force Gun, Model 9000	BFG9000
Colorado School of Mines	CSM
Field flow fractionation-inductively coupled plasma-mass spectrometry	FFF-ICP-MS
Mammoth Armed Reclamation Vehicle	MARV
Stone of Jordan	SoJ

ACKNOWLEDGMENTS

Thanks Mom(s).

This work is dedicated to responsible mining.

CHAPTER 1

INTRODUCTION

The future of underground coal mining is automated. Robotic mining systems will determine optimal work patterns and execute the planned operations with precision. Progress towards this horizon is gradual in the mining industry. Improvements to safety in underground coal mining has been sparse recently, and the National Institute of Occupational Safety and Health (NIOSH) has sponsored programs like this one to accelerate the next industrial revolution. This work focuses on the development of techniques and sensors to automate detection of material type, tool wear, and cutting forces.

Machine operators in underground coal mines are routinely exposed to dark, dusty, noisy, and hazardous conditions. When doing their job of operating the continuous mining machine, they must stand close enough to the cutting interface to infer where they are cutting and if their tools are worn and need replaced. They must also stand far enough away to avoid the dangerous rock cutting process. A well lit and clean view of a continuous miner is shown in Figure 1.1. The long term exposure to hazardous noise and dust causes occupational health issues for miners which work for more than several years.



Figure 1.1 Continous Miner. Pictured is the ‘Remote Continuous Miner HM21 Joy Used for underground coal mining’, originally uploaded to Wikipedia by user Xlxgoggaxlx under the Creative Commons Attribution-Share Alike 3.0 Unported license. The machine operator must stand close to the machine and cutting interface to control the machine. The operators use many cues, but ultimately must track if they are cutting the target material and the state of tool wear. Allowing operators to maintain a greater distance while giving them the feedback they require can improve production and safety. Image Source/License: https://commons.wikimedia.org/wiki/File:Continuous_Miner.jpg

The technologies proposed in this dissertation could be used to automate feedback collection during the rock cutting process, allowing operators to perform their duties from a safer location. This work investigates using measured frequency responses to predict material and wear conditions using a non-linear dynamic capacitive load cell. An acoustic tool wear detection method is also developed using this same premise. The capstone of this project is a custom capacitive load cell that is able to measure rock cutting forces using a linear model. Each of these three works are respectively summarized in the included journal articles.

This work was sponsored by NIOSH contract 75D30119C05413. It is a continuation of prior work at Colorado School of Mines [1]. The previous work employed piezoelectric sensors to make measurements to estimate rock cutting parameters. Our work focuses on use of a capacitive based load cell. Study of rock fracture mechanics [2] and the effects of tool geometry during rock cutting [3–5] have long been pursued to increase mine efficiency and safety. By providing an *in-situ* force sensor, this work provides a means for direct measurement of rock cutting parameters. In addition to enabling operators to perform their roles from a distance, this device could also be used to optimize tool geometries by providing quick and direct feedback of the cutting forces.

The next chapter covers additional background information regarding sensor choice and modelling. The journal articles that summarize the work are included next. After the articles, a chapter which compares the different capacitive sensor implementations is given. An additional chapter describing extensions of the acoustic processing methods is given after that. The journal articles, and this dissertation, have been published as Open Access and are released into the public domain. If you would like implementation advice, you can contact me, the author, at: austinfoftmanns at gmail dot com with the subject line containing "THESIS". I hope you enjoy the rest of this dissertation.

CHAPTER 2

MINING SAFETY BACKGROUND

In the thesis by Moore [4], the author outlines history of mining tools dating back to the 1600s. This is when blasting was introduced to the mining process. Hand tools dominated until the invention of steam powered machines in the mid 1800s. Around 100 years later, at the time of publication of the thesis, compressed air hammer drills were the most popular implement. These techniques and the mining drill bits that they used evolved with each other over time.

The introduction of the continuous mining machine increased productivity and were generally regarded as safe since the operator was enclosed in a shielded cab. Around the 1980s, the remote control for the continuous mining machine led to further increases in productivity. The remote control provides the operator greater visibility of the operation, but at increased risk of injury from the machine or tunnel collapse. The crush hazards from the machine were not mitigated until the introduction of the personnel proximity detector, which prevents the machine from advancing into workers which are wearing the device.

Safety in underground coal mines has not improved over that last decade. Other technologies that have been introduced tend to focus on measuring indicators for collapse after the rock has been damaged such as ... These technologies are reactionary rather than preventative. To prevent hazardous situations from developing, rock cutting must be done with care.

Previous efforts to improve efficiency have tried automating the continuous mining process, but fell short on being able to totally take over for human operators. Experienced operators are an invaluable resource. They have expert knowledge gained through years of working in difficult conditions. Augmenting their expertise with objective feedback and machine precision stands to improve outcomes beyond fully human or fully autonomous control.

Mining safety is really bad and could be improved by moving operators further from the cutting interface. Efficiency can be improved by implementing autonomous process control and feedback mechanisms. To enable these outcomes, we seek feedback mechanisms which can determine quantities of interest for the process. The next chapter discusses sensor technologies that were considered for underground mining.

CHAPTER 3

SENSORS TECHNOLOGY LITERATURE REVIEW

Strain gauges

Piezo

Capacitive

Radio signals

Thermocouple/temp

CHAPTER 4

CLASSIFICATION AND REGRESSION TECHNIQUES

Nonlinear deformation of polyimide films

Motivation for Fourier transform

Dynamic sensor - ζ chaning modees

How classification is done in other domains

physical model for sensors? - described in chapter 10

Linear, Neural Network, SVM... Use an empirical model instead!

CHAPTER 5

LOW-PROFILE CAPACITIVE LOAD CELLS FOR UNDERGROUND MINING MATERIAL AND WEAR CLASSIFICATION TO PROMOTE WORKER SAFETY

This article has been published open access and is part of the public domain.

5.1 Abstract

This work proposes a capacitive load cell for conical picks to enable underground continuous mining machine operators to perform their roles away from known hazardous regions near the machine. The load cell is embedded in commercially available flexible printed circuit board, integrates with the target tooling, and demonstrates in-situ force sensing of vibration signatures for continuous mining cutting tools. Changes in material constitution, tool mass, and tool geometry cause modal variations in vibrational response measurable with force sensors at the cutting interface. Time-series measurements are captured during rock cutting tests using a linear cutting machine. These measurements are segmented into small windows, less than 0.25 seconds, and are preprocessed using the fast Fourier transform, which highlights the modal variations. The transformed measurements are then classified into different material and wear categories using support-vector machines with the radial basis function kernel. Different normalization schemes and Fourier transform methods are tested for signal preprocessing. Results show that the power spectral density measurements with normally distributed coefficients give good results for material classification, while the normalized time-domain measurements give better results for wear classification. Under laboratory conditions, this technique is shown to classify material and wear categories with F1 score above 0.85 out of 1.0 for our experiment. This technology could be used to assist operators in assessing material and wear conditions from a safer distance. It has applications in the coal mining industry as well as other applications which use conical picks such as road milling.

5.2 Introduction

Operators monitoring important process feedback in hazardous regions is dangerous [6]. Operators are expected to monitor machine alignment, tool wear, machine condition, and the material being cut [7]. The hazards that the operators are exposed to in underground mining can be difficult to model [8]. To allow operators to perform their role from a greater distance, we propose a sensor suitable for assisting operators in assessing material type and tool wear that integrates with conical picks on continuous miners used in underground coal mining.

Underground mining is dangerous and safety has not been improved over the last decade, with fatalities per 100,000 full time equivalent employees averaging 21.4 from 2011-2020 [9]. In particular, coal workers are roughly 50% more likely to be injured than workers in other mining sectors and account for roughly 50% of fatalities from 1983 to 2020[9]. Existing technologies for mitigating these hazards monitor the environment with micro-seismic sensors, distributed pressure sensors, or electromagnetic analysis [8]. These technologies only identify hazards after they occur. Elimination of hazardous conditions is the most effective method for reducing risk to workers in any application [10]. The only way to eliminate these hazardous conditions is to allow the operators to perform their role from a greater distance.

Previous efforts to allow operators to perform their role from a greater distance, namely development of remote controls, have allowed operators to collect better visual feedback; however, operators often put themselves in hazardous positions to do so [11]. Technologies also assist operators by automating some tasks. For example, automated hydraulic diagnostic systems can help operators monitor the machine's hydraulic conditions [12]. One of the most effective technologies for reducing worker injury is the personnel proximity detector, which disables certain machine operations if designated zones near the machine are entered by persons tracked with the device [13]. This device was implemented about a decade ago; however, there have not been any major improvements since.

Direct measurements of rock and pick interaction have previously noted significant differences in forces between tool wear levels [14, 15]. Material has been differentiated by vibration signatures using various classification techniques as early as 1993 [16]. Previous efforts for smart bit or intelligent pick tooling to perform these tasks in real-time during operation have taken place over the last few decades, examples include: using neural networks to classify tool wear in potash [17], using acoustic data to classify both material and tool wear in coal cutting [18], using piezo sensors to deduce rock chipping [19], and, most recently, using an instrumented block with integrated strain gauges to measure cutting forces [20]. So far, results using capacitive load cells have not been found for material and tool wear classification in underground mining. Advances in both capacitive sensing and vibration classification have unearthed a variety of applications in other domains. Our sensor, shown in Fig. Figure 5.1, can assist operators in assessing material type and tool wear by measuring differences in vibrational responses between the different conditions.

To test our sensor for material and wear classification, full-scale rock cutting experiments are performed using the linear cutting machine at Colorado School of Mines, a popular type of tool for rock cutting mechanics testing [21]. A limestone sample cast in concrete is used to test material classification. Conical picks of three different wear levels at an attack angle of 45 degrees are used for tool wear classification. The wear levels are *new*, *moderate*, and *worn*, where *moderate* represents a pick halfway through its useful life,

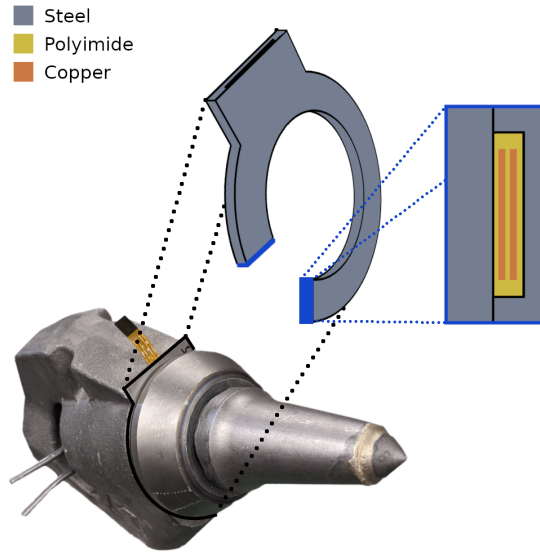


Figure 5.1 A prototype of the sensor integrated with the U92 4.0 22NB Conical Pick and K35 Block system, from Kennametal. The device is shown without the measurement collection system and is situated between the sleeve and the block. The FlexPCB interface is exposed, which provides access to the capacitive sensors' electrodes. A steel case protects the FlexPCB sensor and provides the necessary stiffness to transfer the input forces to the sensor. An embedded electronics platform, not shown in this figure, takes measurements suitable for dynamic classification of tool-wear and material. A cutaway of the sensor shows the thin film design for the force sensor.



Figure 5.2 The different pick wear levels. The *new*, *moderate*, and *worn* pick tips have spherical diameters of 3.71 mm, 17.9 mm, and 27.5 mm respectively. This approximates an even wear pattern. The *moderate* and *worn* tips were artificially worn using a lathe.

and *worn* is a tool at the end of its useful life. The tool tips are artificially worn to a spherical diameter using a lathe to approximate an even wear pattern and for reproducibility. A closeup view of the tool tips and the values for their spherical diameters is shown in Fig. Figure 5.2. The low profile sensor sits between the sleeve and block. The sleeve has been machined down to a slip fit in the block to allow force transfer to the sensor. The sleeve and block are both retained by a large pin. Measurements are collected from the sensor using an embedded capacitance to digital converter and sent to a computer over USB.

To highlight the changes in vibrational modes, the data is transformed using short window fast Fourier transform preprocessing before classification. The resulting vectors are classified into material and wear categories using the support-vector machine technique. Data from strain gauges embedded in the linear

cutting machine and our custom sensor are both used on their own for classification. Each classification system in our experiment is scored using the F1 score [22, 23]. The best performance for material and wear classification yielded F1 scores around 0.85 out of 1.0 for our experiment. Performance in tool wear classification is shown to be comparable between the custom sensor and the strain gauges embedded on the linear cutting machine. For material classification, the additional sensitivity due to the proximity of the custom sensor to the cutting interface allows it to perform better using the same algorithm.

The rest of this article is organized into sections. First, background information regarding material and wear classification algorithms is given along with a description of the algorithm we use. Then, the sensor design and characterization is described. After, the procedure for the rock cutting experiment is given, followed by the performance results of the classification algorithm. Finally, some discussion points and conclusions regarding the experiment and results are shared.

5.3 Material and Wear Classification

Material identification techniques for rock cutting can use metrics based in force and energy measurements, as different rock materials are known to require varying energy to break down [24, 25]. For tool wear classification, force or vibration feedback is commonly used in other domains such as metal milling or oil drilling because changes in tool mass and geometry cause the vibrational modes to shift [26–29]. Both material and tool wear classification can be framed as a vibration classification problems. Vibration classification lends itself towards certain standard signal processing and classification techniques, primarily with frequency domain preprocessing [30].

Preprocessing the input sensor data using different spectral or statistics based methods to improve classification results is popular [28, 29, 31, 32]. For this research, the fast Fourier transform is chosen as the preprocessing technique as it has been shown to give good results in many domains [33]. Depending on the chosen kernel for the support-vector machine, data standardization can range from beneficial to necessary, as the kernel may be built with assumptions on data mean values and range. The effects of the chosen normalization and preprocessing methods, or their absence, on the classification results are explored in this work.

The classification technique used after preprocessing is the support-vector machine (SVM) using the default ‘C-Support Vector Classification’ implementation in the Python library Scikit Learn [34], [35]. SVM has long been known to be able to classify model behaviors [36]. It has also shown useful specifically in tool monitoring [37]. In general, the SVM works by finding a hyperplane in the data set which separates the data into the prescribed categories then, this hyperplane can be used as a quick decision rule for classification of future inputs [34]. The advantage of the SVM is it first transforms the input data to a

higher dimension using a kernel function which helps to separate the data. This method has few hyperparameters and is considered generalizable, only needing relatively little training data to achieve good performance.

The SVM technique has few hyperparameters when compared to other machine learning techniques like feed-forward or convolutional neural networks, which allows it to be implemented quickly and be generalizable. The SVM is also typically better performing than simple techniques like k-nearest neighbors. K-nearest neighbors is another popular and low hyperparameter technique for vibration classification, and it works by selecting the majority class of the ‘k’ samples closest to the input in its memorized training data [38]. The SVM solves the classification problem in a similar way, but reduces the training data for computational efficiency and better sensitivity to general trends. More advanced techniques, such as feed-forward or convolutional neural networks, are flexible techniques for vibration classification that work by numerically optimizing a series of weighted vector functions to approximate the statistical likelihood of a given input being from each output class based on the training data [39]. SVM strikes a balance between these techniques as it generally has better performance than k-nearest neighbors but is not as prone to over-fitting as the feed-forward or convolutional neural network.

5.3.1 Classification Methods

Time-series measurements are recorded from the four channels of our custom sensor and the four channels of the strain gauges on the linear cutting machine. For either sensor, we denote these measurements as $CH_x[n]$, where x is the channel index ranging from 1 to 4 and n is the sample index ranging from 1 to T , the total number of measurements. These time-series measurements from each sensor are then chopped into small segments representing short duration (≤ 0.25 s) windows of signal. These discrete vectors are preprocessed to form the feature vectors to be classified by the support-vector machine. For an individual classification sample, the data from a particular channel can be denoted as $\overrightarrow{C_{kx}} = [CH_x[k], CH_x[k+1], \dots, CH_x[k+M-1]]^\top$, where k is the index corresponding to the start time of the sample window, x is again the channel index, M is the number of samples in the window, and $[\cdot]^\top$ represents the matrix transpose operation.

Both window overlap and window size are varied during our tests to observe their effects on performance. Increasing window overlap generates more data vectors for training and testing, but the resulting samples are more redundant than those generated with less overlap. Increasing window size gives data with more features which can improve classification accuracy. The classification rate is limited to one classification per window, and windows may overlap to increase the rate. A short window which gives acceptable performance is desired for rapid classification suitable for real-time use.

Each point in time can be assigned a class label for both material and wear. Only windows with contiguous labels are used in the experiment. Samples which are near the beginning or end of a material are discarded, as they do not have a clear ground truth label and are not representative of the steady state cutting dynamics. Separate classification systems are trained to identify material and wear. For an individual classification experiment, the set of paired measurement and class data is split randomly into testing and training sets. The set with the training indices is denoted in this work as R , while the set of testing indices is Q . After being windowed and split, the feature vectors for classification via support-vector machine are represented as:

$$\vec{X}_i = \mathcal{P}_\theta \left(\begin{bmatrix} \vec{C_{k1}} \\ \vec{C_{k2}} \\ \vec{C_{k3}} \\ \vec{C_{k4}} \end{bmatrix} \right), \quad (5.1)$$

where \mathcal{P} is the preprocessing pipeline for the data and θ are the parameters fit from the samples in the training set. The subscript, i , is the sample index and ranges from 1 to N , the total number of vectors in the data set. The specific mapping between i and k depends on the window parameters. The Scikit ‘sklearn’ library [34, 35] provides a convenient data structure, the Pipeline object, which encapsulates these steps for consistent application and ensures that data from the testing set is not used during parameter fitting.

For our experiment, the pipeline consists of the composition of three optional operations, detailed in Table ??, and discussed here:

$$\mathcal{P}_\theta = \mathcal{N}_\theta^2 \circ \mathcal{F} \circ \mathcal{N}_\theta^1 \quad (5.2)$$

where \circ represents the function composition operator. The steps denoted with \mathcal{N} are normalization steps which transform the input data to be zero mean and unit variance along each feature using the sample mean and variance from the training set. The \mathcal{F} operation is the frequency based transform, and different variations of the fast Fourier transform are used. Every combination of processing steps is used, and the results are compared to determine the best methods for this application. Each step is also substituted with the identity function during this process as a control.

In addition to the preprocessing step, the support-vector machine also can apply a transform to the input data during its use. A description of the support-vector machine algorithm, adapted from [40] is given here. Intuitively, the support-vector machine finds a hyperplane between two sets of data. This is done efficiently by representing the hyperplane as a linear combination of a subset of the training data.

Table 5.1 Preprocessing Pipeline Steps, $\|\cdot\|$, \cdot^2 , and $\sqrt{\cdot}$ are element-wise absolute value, square, and square root respectively.

Symbol	Values	Description
$\mathcal{N}_\theta^1, \mathcal{N}_\theta^2$	StandardScaler	$\mathcal{N}(\vec{X}_i) = (\vec{X}_i - \text{mean}(\vec{X}_i)) / \text{std}(\vec{X}_i)$
	None/Control	$\mathcal{N}(\vec{X}_i) = \vec{X}_i$
\mathcal{F}	FFTMag	$\mathcal{F}(\vec{X}_i) = [\ FFT(\vec{C}_{k1})\ , \dots, \ FFT(\vec{C}_{k4})\]^\top$
	FFTSQ	$\mathcal{F}(\vec{X}_i) = [FFTMag(\vec{X}_i)]^2$
	FFTSQRT	$\mathcal{F}(\vec{X}_i) = \sqrt{FFTMag(\vec{X}_i)}$
	None/Control	$\mathcal{F}(\vec{X}_i) = \vec{X}_i$

These vectors from the training data are known as the support vectors. The binary classification support-vector machine works by solving the primal problem:

$$\min_{w, b, \xi} \frac{1}{2} \|w\|^2 + C \sum_{i \in R} \xi_i, \quad (5.3)$$

$$\text{s.t. } y_i [w^\top \phi(\vec{X}_i) + b] \geq 1 - \xi_i, \quad \forall i \in R. \quad (5.4)$$

$$\xi_i \geq 0, \quad \forall i \in R. \quad (5.5)$$

where w and b are the vector and offset representing the decision boundary hyperplane, ξ_i are slack variables which allow for error in classification in case of an infeasible problem. The y_i are binary class labels with value -1 or 1, C is a regularization parameter, and $\phi(\cdot)$ is an implicit function which transforms the feature vectors into a higher dimension before separation with the hyperplane. The function $\phi(\cdot)$ is implicit because in practice the dual of the primal problem is solved and only the inner product of the transformed input vectors is computed. This is done with the ‘kernel trick’, whereby a kernel function, $K(x, y) = \langle \phi(x), \phi(y) \rangle$ is used, which is less costly to compute than the full inner product in the higher dimension. After solving the dual problem, the decision function for an unseen sample, \mathbf{x} is given by:

$$y_{pred}(\mathbf{x}) = \text{sgn} \left(\sum_{i \in S} \alpha_i y_i K(\vec{X}_i, \mathbf{x}) + b \right), \quad (5.6)$$

where the α_i are the new coefficients given from the dual formulation and S is the set of support-vector indices. It is noteworthy that the final decision function does not explicitly use the hyperplane as represented by w , but instead relies the offset variable b and dot products (through the kernel) with the training data. To use the support-vector machine for multi-class problems, the chosen implementation uses a ‘one-vs-one’ voting scheme where a binary classifier is trained for each pair of class combinations. The class with the lowest index and most votes is chosen as the output.

The radial basis function is a popular kernel choice, as it was one of the first to be developed. It is similar in function and performance to using auto-correlation as the implicit function [41]. Since the radial basis function gave acceptable performance and to limit the number of hyperparameters, only it is used for this study.

To test our classification system, the feature vectors are sorted into testing and training sets using ratios of 25:75, 50:50, 75:25. Each split is done randomly, 100 times, for each combination of preprocessing parameters. Hyperparameters for our method are window duration, window overlap ratio, and window shape. Window duration is set to 0.05, 0.10, 0.15, 0.20 and 0.25 seconds, while overlap ratio is set to 0.25, 0.50, and 0.75. The window shape is left as rectangular for the entire study. Ringing effects from frequency convolution with the $\text{sinc}(\cdot)$ shape of the window in the frequency domain will be applied consistency across samples. Discovery of the optimal window shape would require it's own extensive hyperparameter study across the many popular window functions. To limit the scope of the study, and since adequate performance was given with the rectangular window, focus is given to the other hyperparameters.

The effect of the preprocessing steps or their absence is investigated for this classification system across the hyperparameters of window size and overlap. Each classification setup is scored using the F1 score [22, 23] which is the harmonic mean of the classifiers precision and recall:

$$F_1 = 2 \frac{\text{precision} \cdot \text{recall}}{\text{precision} + \text{recall}} \quad (5.7)$$

Precision is the ratio of positive classifications that are correct while recall is the ratio of positive samples which are correctly identified [23]. The F1 score provides a numeric value between zero and one, with one being a perfect score. For our multi-class problem, we train the SVM using the ‘balanced’ strategy where classes are given equal weight, regardless of class samples size, by setting regularization term, C , inversely proportional to the class frequency in the input data. We score the classifier using ‘macro’ averaging for the F1 score where the final score is the unweighted average of the F1 scores for each class. Using this setup, the classifier is trained to give equal weight to each class type, regardless of population size, and classification performance and is scored with a metric which also gives equal weight classifier performance for each class. Additionally, confusion matrices and accuracy measurements are used to get a more complete sense of classifier performance.

From this study, the optimal subset of steps may be found in a verifiable way. The training and testing computations are performed on the Isengard supercomputer at Colorado School of Mines. Individual classifiers can be trained on a consumer laptop in less than a minute, but to run the thousands of tests for this study in a batch manner, the supercomputer is more appropriate. For each set of parameters, the mean

and standard deviation of the F1 scores are recorded for a population of 100 experiments with different random splits of data. Setups giving scores with large deviations or high dependence on the test and train ratio are suspect for overfitting to non-relevant features in the data set, while a low deviation with a high mean F1 score that is similar across test and train ratios can be considered generalizable and useful for the target application. To meaningfully compare distributions of scores generated for each method, the Welch-Satterthwaite method (Welch's t-test) is used to determine if differences are significant [42]

5.3.2 Sensor Design Literature Review

When it comes to designing a sensor for underground mining applications, there are several key constraints: the device must be low power, low cost, and highly durable. Capacitive sensors generally meet these requirements. Sensors that are not considered directly for this study are Inertial Measurement Units (IMUs) or custom microelectromechanical systems (MEMS) devices due to their power consumption, cost, and fragility. The most promising fabrication technology found during our literature review was capacitive load cells embedded in flexible printed circuit boards. The sensor dynamics can be non-linear, so the collected measurements are compared to those of a linear force sensor.

Capacitive pressure sensor designs have used steel enclosures [43], film dielectric [44], and sensors made directly from flexible circuits [45]. Larger film dielectrics can be modeled with a general system of springs and dampers; however, with thin films only a few dozen μm thick, the molecular dynamics contribute greatly to the response [46] and make it non-linear. Encasing the flexible circuit element in an enclosure provides a rigid structure with more linear deformation, but the dielectric still affects the relationship between the input force and the measured capacitance. These flexible sensors are low in cost, while sensors which provide more linear measurements normally employ careful manufacturing processes, air gap designs, and different signal processing techniques such as those seen in [47–51]. Sensors which use thin films with non-linear deformation must use appropriate models and algorithms to achieve the desired classification results.

Popular flexible dielectric materials like carbon-doped thermoplastic poly-urethane and silicone can exhibit non-linearity through hysteresis, viscoelastic effects, or measurement creep [52–55]. The choice of dielectric material for a capacitive sensor will influence much of its performance, so it is important that the material have robust properties for the expected range of conditions. Polyimide is a notable flexible dielectric material and sensor substrate for capacitive sensors due to its high temperature range, solvent resistance, and low surface roughness [56]. It is also easily integrated with electronic circuits boards, known as flexible printed circuit boards, where it serves as the substrate for conductive traces. However, when used in a thin film, polyimide has nonlinear deformation dynamics due to the complex molecular

interactions of the constituent polymer chains [57]. This viscoelastic-plastic behavior can be difficult to model for a large range of input, with models either incorporating complicated numerical integration techniques [58, 59], only capturing the linear viscoelastic portion for small ranges [60], or ignoring the unloading phase [61]. Thicker films generally have a greater linear range [62] and most models incorporate some mix of viscoelastic and viscoplastic elements like the model seen in [63].

Other works which have used polyimide as the force or pressure sensor dielectric show mixed results for sensor performance. In one study, electrospun polyimide nanofibers were used as the dielectric to achieve measurement repeatability and sensitivity [64]. When the device was cycled from 0 to 10 % change in nominal capacitance for 10,000 cycles, no noticeable measurement creep was observed. In another study, spin coated polyimide was used, and the sensor response was much noisier and subject to some initial transient effects [65]. Another group used a FlexPCB force sensor encased in polymeric materials and it showed good linearity and low hysteresis for 1% changes in capacitance [66]. These studies indicate that polyimide is a good low-cost material choice that can still give good performance.

5.3.3 Sensor Design

To design a capacitive force sensor for material and wear classification, suitable choices must be made for materials, geometry, and the balance between sensor accuracy and bandwidth. Based on the sensor design literature review, a steel case with a load cell embedded in a flexible polyimide circuit board is chosen for the design. The steel is 303 series stainless, chosen to reduce potential for corrosion and for its resistance to fatigue. The steel case is made by chemical etching of 0.036 inch steel plates. A channel of 0.018 inch depth is formed on one plate and the two are laser welded together after a steel shim and the sensing membrane have been put in place. As noted in the prior section, polyimide is chosen for the sensing membrane for its wide range of operating conditions and robust properties. The sensor case geometry is largely determined by the target tooling, but must still be tuned to the operational requirements of the sensor. Likewise, the balance between sensor accuracy and bandwidth must be tuned to achieve the desired results.

To tune the case geometry for the desired stiffness, appropriate values must be chosen for the thickness and height of the side walls. These values are shown as \mathbf{h} , \mathbf{w}_1 and \mathbf{w}_2 in Fig. Figure 5.3. The donut shaped sensor has a center filled with viscous polyimide. The thickness and height of the side walls chiefly determines the spring constant of the sensor. The polyimide is much more compliant than the surrounding steel, so the overall case deformation is not influenced by its deformation in a significant way. However, the capacitive cells are directly embedded in the polyimide, so the measurement is greatly influenced by its deformation.

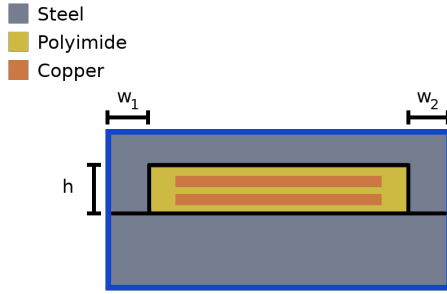


Figure 5.3 A cutaway of the sensor with the geometric parameters shown. The dimensions of the walls may be tuned to give the sensor the appropriate stiffness. The thickness of the top and bottom plates do not significantly influence the overall stiffness of the device.

The sensor is designed for a maximum expected force of 200 kN. This provides some margin above the expected forces, which can be in excess of 100 kN for hard rocks. The sensor case is tuned to have around 10% strain at maximum load, in this way material fatigue can be mitigated and the measured capacitance should be close to linear with dielectric deformation. The thickness and height of the side walls, h , w_1 and w_2 are set to about two and a half millimeters. The deformation of the steel case is expected to be mostly linear within this range of deformation.

The balance between sensor accuracy and bandwidth is determined by the range of deformation of the sensor as well as the capacitance and resonant frequency of the sensing circuit. In general, larger capacitance values will provide greater accuracy at the cost of sensor bandwidth. For the chosen hardware, the effective number of bits for the measurement is proportional to the square of the measurement time. Larger capacitances take longer to settle but can make more accurate measurements.

Given the tool geometry, four cells are placed in the donut: two large and two small. For our parallel plate design, it is important that the electrodes receive even loading, otherwise the parallel plate approximation is no longer valid. The large cells are designed for a nominal capacitance of 541 pF and the small cells are designed for a nominal capacitance of 412 pF. All four pads occupy about 50° and are spaced evenly around the donut. The larger cells have about 30% greater area.

Since we are focused on high-frequency vibration classification, sensor bandwidth is maximized while still providing sufficient resolution and accuracy for classification. At a rate of 400 samples per channel per second, and using a gain of 4, the embedded system is able to provide 128 levels for up to a 25% change in capacitance. At 10% max expected deformation, the max expected change in capacitance is also about 10%. The true deformation of the polyimide around the electrodes is nonlinear and must be characterized

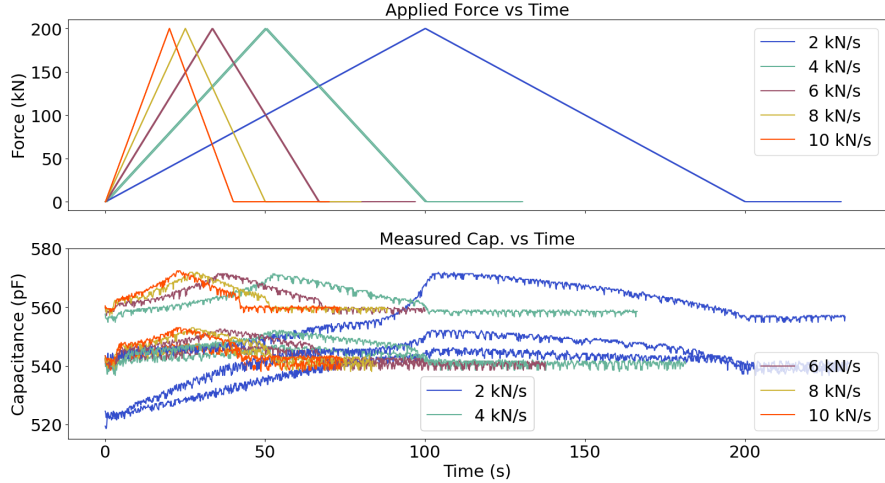


Figure 5.4 The triangular load profiles and the resulting measurements from the sensor. The sensor response is not symmetric and therefore non-linear. Lower load rates cause greater changes in displacement, which is consistent with previous studies for thin film polyimide.

to make informed decisions with the resulting measurements.

5.3.4 Sensor Characterization

The sensor was characterized using load frame testing. Five different load rates were applied to three separate sensors to achieve a max force of 200 kN momentarily before ramping back down at an equal rate. Linear sensors show symmetric behavior for such a test, but the sensor measurements for this test, shown in Fig. Figure 5.4, reveal that our sensor exhibits hysteresis and rate dependence for these loads. These effects can be expected from the previous literature regarding polyimide deformation [56–66], and they obscure the effect of the average force on the measurement. It can be seen that, as the loading rate increases, the traces converge. This implies that the sensor can still be used to detect the changes in the high frequency components of the response that are useful for vibration classification. The overall deformation of the sensor case during these same loads is shown in Fig. Figure 5.5, and the deformation is linear. This confirms that the nonlinear deformation is happening in the polyimide and suggests that this case could be used to house other sensing technologies that can transduce displacement to electrical signals.

5.4 Rock Cutting Experiment

To test the sensor for *in-situ* force signature capture, rock cutting experiments were performed using the Linear Cutting Machine in the Earth Mechanics Institute at the Colorado School of Mines. A limestone sample cast in concrete was cut using a conical pick on the instrumented block. Time series

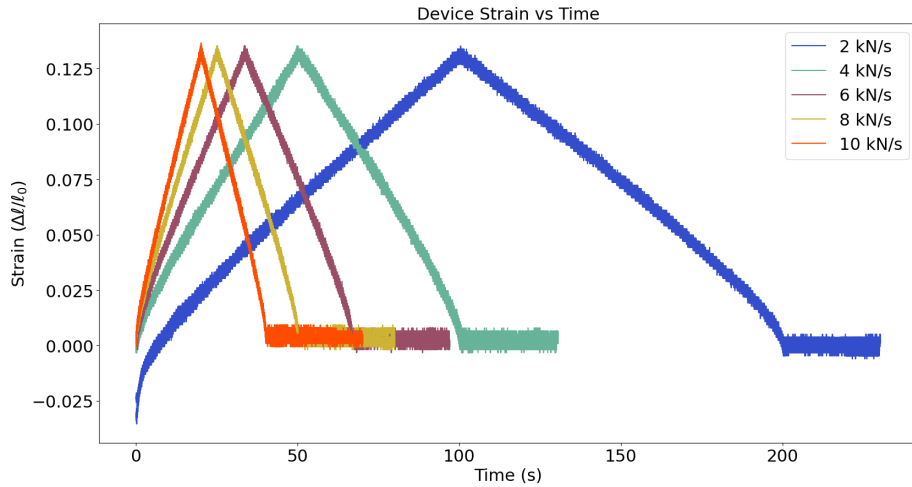


Figure 5.5 The case deformation during the load frame tests. The case deformation is symmetric for the loading and unloading phases, it also has a consistent slope for force over displacement. This means the case has approximately linear deformation for these load profiles.

measurements were made with the custom sensor as well as strain gauges integrated with the test equipment. The measurements were cut into small intervals and used with the classification algorithms to build separate material and wear classifiers

To capture the capacitive measurements, a capacitance to digital converter made by Texas Instruments is used: the FDC2114. This device interfaces with a generic microcontroller over I2C, a popular circuit to circuit interface. The software used on the microcontroller is available on Github as well as the data-acquisition software which is ran on the host computer to collect the measurements. The software that performs the classification experiment described in the previous section is also available. The microcontroller code is available here: <https://github.com/Fworg64/DAQuery>. The data-acquisition code is available here: <https://github.com/Fworg64/reDAQ>. The machine learning and classification code is available here: https://github.com/Fworg64/limestone_experiment.

The Linear Cutting Machine, shown in Fig. Figure 5.6, uses hydraulic actuators to drag the sample against the cutting tool. A cutting speed of 10 inches per second was used, which is relatively slow compared to the cutting speeds used in the field. The integrated strain gauges measure forces at a rate of 537.6 samples per second. The custom load cell makes measurements at a rate of 400 samples per second. The measurements from each sensor were recorded for use in the classification experiments. For applications with greater cutting speed and more materials, consider that rock fracture is largely static and machine vibration is dynamic. The frequency domain features associated with tool wear should scale with

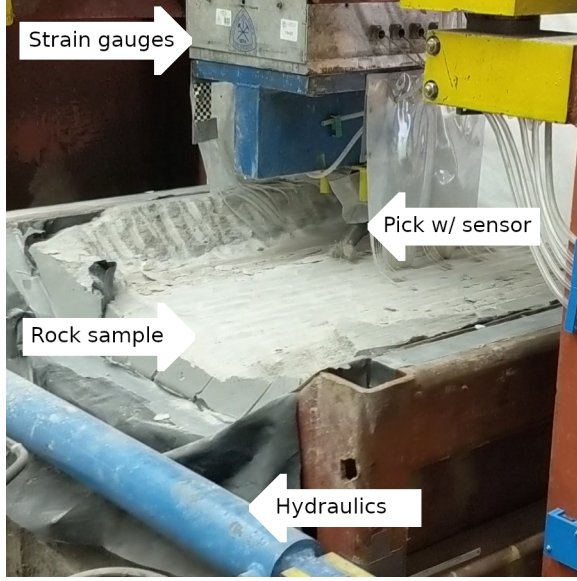


Figure 5.6 The Linear Cutting Machine in action. Hydraulic actuators push the sample into the cutting tool while the custom sensor and the embedded strain gauges record measurements. The tool is normally surrounded by the plastic curtain to aid in capturing dust for a simultaneous study of the effect of tool wear on dust generation.

cutting speed and depend largely on the machine's natural modes, while those associated with material breakdown occur at much higher frequencies.

5.5 Classification Results

Using the method outlined in Section 2, the collected data is used to train and test the classification algorithm. The capacitive sensor data gave results similar to the linear sensor in tool wear classification. For material classification, the capacitive sensor generally performed better. The distribution of feature vectors, before being processed with the support-vector machine kernel, are shown for both sensors by material in Fig. Figure 5.8 and by tool wear in Fig. Figure 5.9. From these distributions, it can be seen that the capacitive sensor is much more sensitive to the higher frequency components of the interaction forces. This is likely a result of its closer proximity to the cutting interface. Typical measurements from cutting experiments are shown in Fig. Figure 5.7.

For each sensor and application, five window sizes were tested. This gives ten pairs for comparison among each group of five, so we choose $p < 0.01$ as statistically significant for differences in performance. The distributions of F1 scores for the classifiers with different window sizes are shown in Fig. Figure 5.10. For tool wear classification, performance was similar for all window sizes for both sensors. For material classification, the capacitive sensor gave measurements which could be more reliably classified. The differences in performance across window sizes are significant for material classification with either sensor.

Classification scores broken down by technique for the 0.2 second window size are shown in Fig. Figure 5.11. Trends in relative method performance were the same across window sizes. It was found that normalization after transformation, and not before, gave the best performance for the Fourier based methods. Also, the normalized time-series data with the SVM gave the best performance for tool wear classification in both the strain gauge and capacitive sensor cases. For material classification with the strain gauges, most methods gave similar performance. Normalization improved classification performance in nearly all categories.

Overall, tool wear in our data was classified with greater accuracy than material type. For tool wear, the normalized time domain data gave better classification results than the frequency data. For material type, only the capacitive sensor gave results that would be useful. The strain gauge data was classified with about 50% accuracy by the classifier. With the capacitive sensor classification of material type, performance using the frequency based data gave slightly better accuracy than the time domain data.

When using only 25% of the data for training, the classifier was still able to perform reliably using the capacitive sensor data. This shows that performance was not very dependent on the test and train ratio. F1 scores with standard deviations are given for the best setup for each application at different test and train ratios in Table Table 5.2. The scores do not change by a large magnitude, which indicates that the classifier is general and should perform well for larger data sets.

Individual confusion matrices are given for the 25:75 test and train ratio for material classification in Table Table 5.3 and for tool wear classification in Table Table 5.4. For these confusion matrices, rows represent the true class for the samples and columns represent the predicted class. Diagonal entries represent correct classifications, and each column is normalized to the number of predictions made of that class. The strain gauge material classifier has poor precision for concrete samples, as many of its concrete predictions are actually limestone samples. The F1 score is sensitive to this, and it is reflected in the much lower score. The accuracy of the strain gauge material classifier is around 80%, which is still useful. The accuracy of the capacitive sensor material classifier is higher, above 95%. This highlights the importance of using multiple metrics to accurately assess classifier performance.

Table 5.2 Scoring metric and test/train ratios for each application

F1 Scores (mean \pm std. dev., 100 trials)			Test and Train Ratio		
Application	Sensor	Best Config.	25:75	50:50	75:25
Tool Wear	Cap.	Time Domain	0.971 ± 0.003	0.965 ± 0.003	0.950 ± 0.004
	SG	Time Domain	0.955 ± 0.005	0.947 ± 0.004	0.934 ± 0.004
Material	Cap.	FFTMagSq	0.924 ± 0.053	0.902 ± 0.044	0.831 ± 0.085
	SG	FFTMagRt	0.533 ± 0.045	0.536 ± 0.026	0.534 ± 0.016

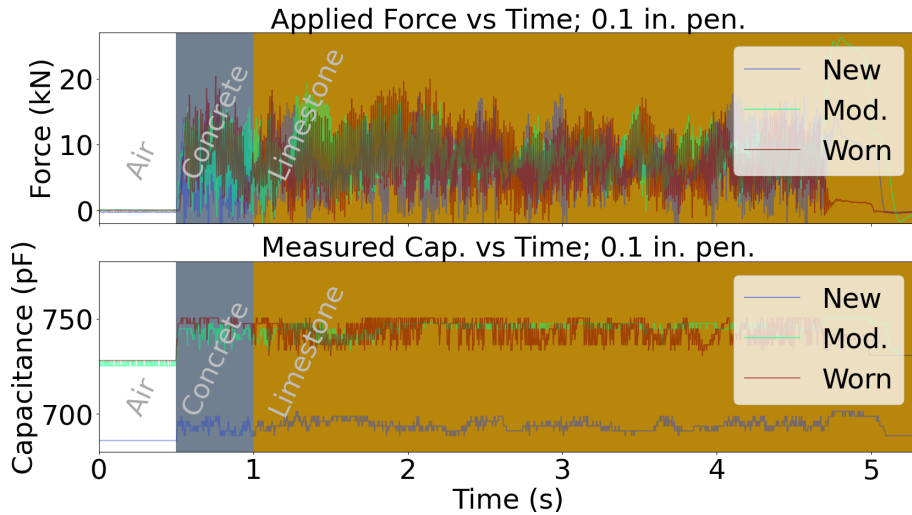


Figure 5.7 Measurements for typical rock cuts with different tool wear levels. The measurements from the linear sensors are shown in the top graph while the measurements from the custom sensor are shown below.

Table 5.3 Confusion Matrix for Material Classifier; Normalized by prediction
New Picks, 0.3 in Penetration, 0.2s Window, 50:50 test and train, PSD w/ post norm.

% Pred.	Strain Gauge Prediction		Cap. Prediction	
	True Class	Concrete	Limestone	Concrete
Concrete	0.117	0.000	0.923	0.013
Limestone	0.883	1.000	0.077	0.987

5.6 Discussion

Our sensor, as used in our experiment, shows promise as a method to objectively assess material type and tool wear. Under laboratory conditions, the sensor and classification scheme was able to detect differences in mode excitation caused by different materials and tool wears. For our experiment, the materials chosen were limestone and concrete. These materials are both much stronger than coal, but our experiment shows that they excite distinct modes in our cutting equipment. For tool wear, it is known that more worn tools can require several times the force to cut when compared to a new tool. The modes that are excited in the machine also change based on the changing tool geometry. For the target application of coal mining, coal is known to be much weaker than the material in which it is embedded, e.g. limestone. So, if our sensor is able to differentiate between concrete and limestone, it is postulated that it could differentiate between limestone and coal, which is much softer.

Using the Support-Vector Machine, the hyperplane between the measured datasets is found. This means that for a given input of discrete frequency or time samples, each value is multiplied by a coefficient

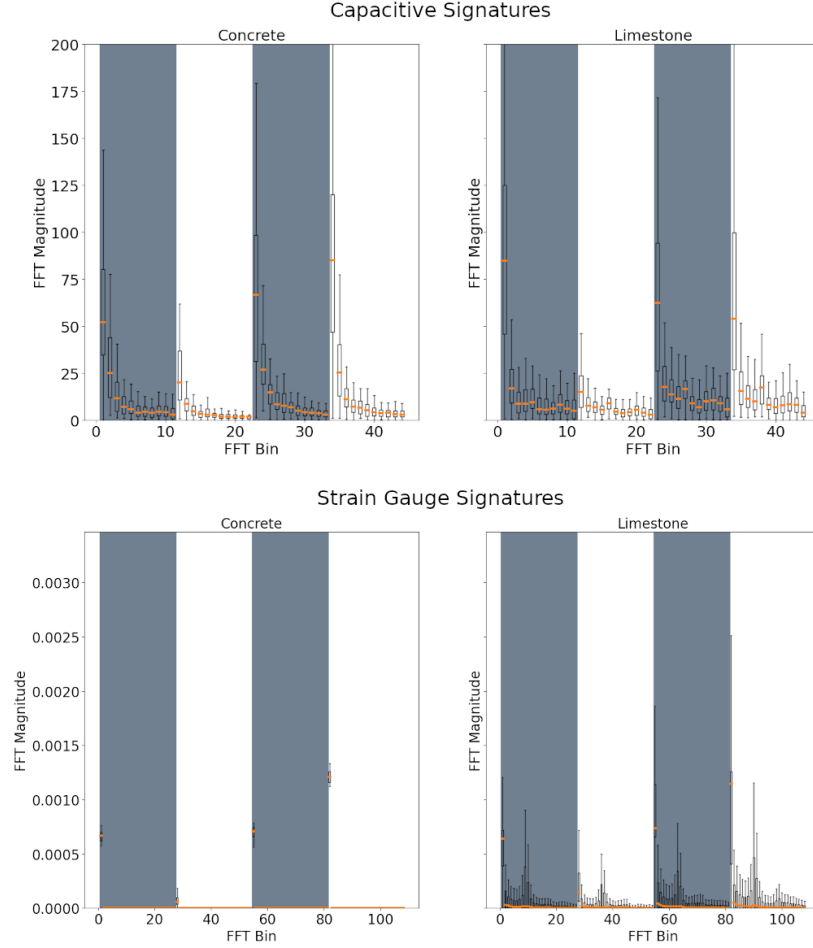


Figure 5.8 The frequency signature distributions collected from the custom sensor organized by material. The concrete material shows exponential decay after each primary mode, while the limestone has a more varied response. These differences can be used for classification of the signals by material.

and then combined to a single value, similar to a digital filter. The Support-Vector Machine has few hyperparameters, and the chosen measurements are shown to contain modal shifts that correspond with the categories of interest. The fundamental change in signal occurs as a mode distribution shift. This is readily detected by the Support-Vector machine.

To adapt our sensor to the target application, the target machine would need to be characterized in terms of dynamic modes. The sampling rate of the sensor system will need to be sufficiently higher than the primary modes of the target tooling, otherwise the measurements could be subject to aliasing. So long as the sampling rate at least satisfies the Nyquist criterion for the tool primary modes, aliasing should be minimized due to the high frequency attenuation caused by massive mechanical systems. Further, the

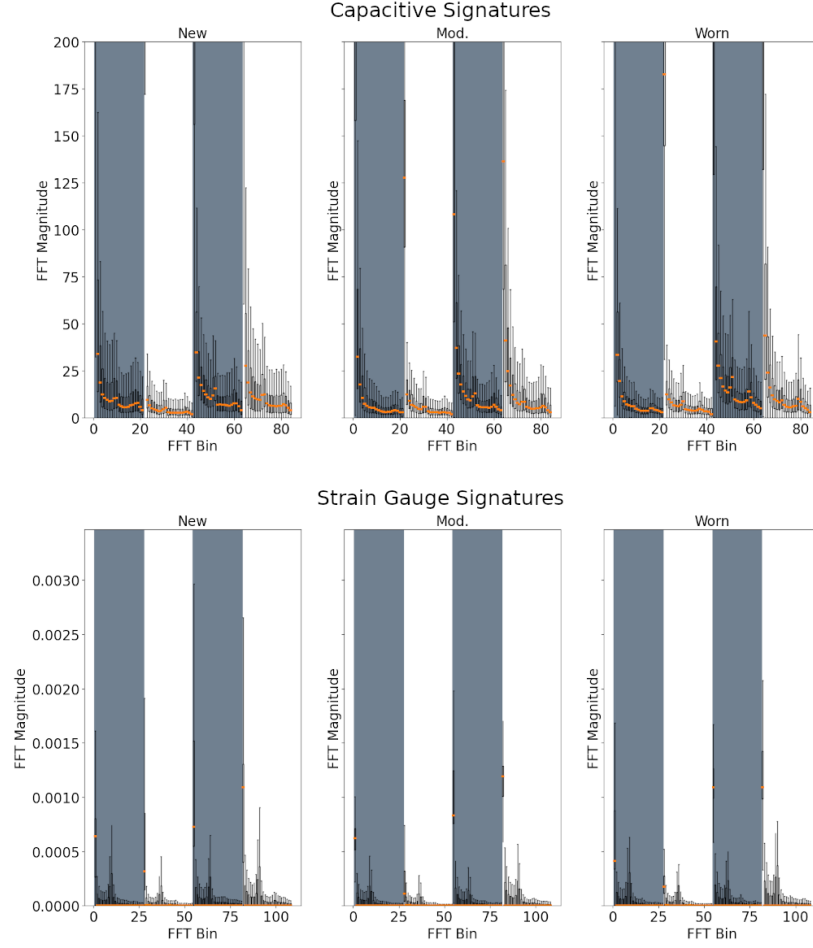


Figure 5.9 The frequency signature distributions collected from the custom sensor organized by tool wear. The New tool has a distinct response compared to the Moderate and Worn tools, and the energy in the higher modes generally increases with wear. These differences can be used for classification of the signals by tool wear.

viscous nature of the polyimide sensor provides even more damping, reducing the possibility for aliasing at the physical level.

Additional sensor designs such as an air-gap capacitive displacement sensor should also be investigated, as they could likely achieve more linear measurements at the cost of sensitivity. Development of a suitable power source and communication system must still be considered for this application. Other technologies such as acoustic sensors also show promise for material and wear classification, as they have been used with success in other domains and acoustic information is one of the primary feedback mechanisms currently employed by operators. A load cell based technology would likely be less susceptible to outside interference

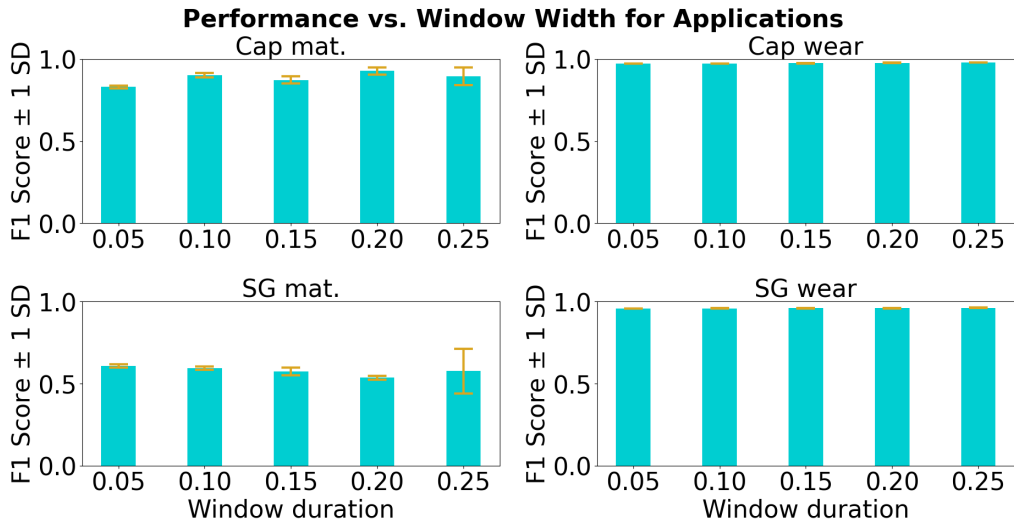


Figure 5.10 Bar chart with error bars for F1 score distributions by window size. For tool wear, both sensors were able to provide sufficient data for very accurate classification. For material classification, the capacitive sensor generally performed better than the strain gauge sensor. Some of the differences in performance are significant within the application and sensor combinations, but in general performance was similar across window sizes.

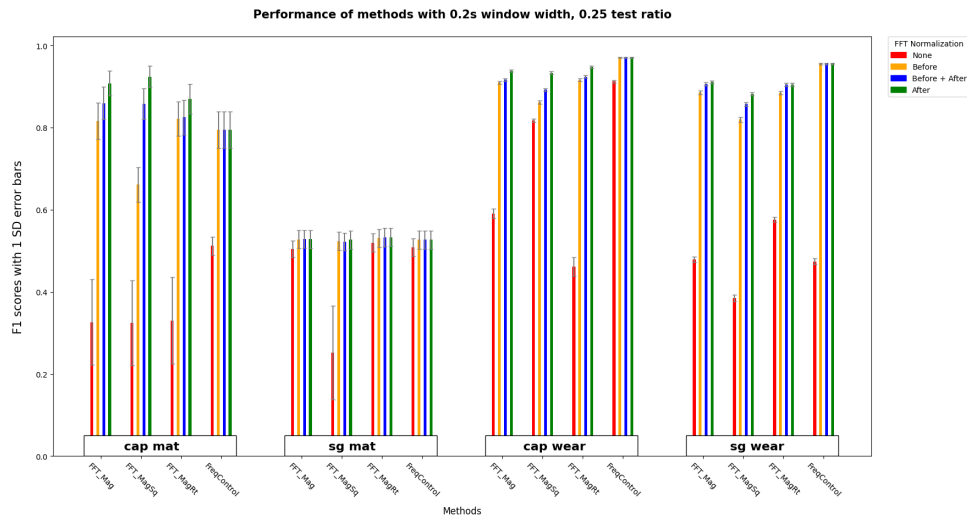


Figure 5.11 Performance of different preprocessing methods for each application. In general, normalization after transformation proved most effective for the frequency based techniques. Using the normalized time domain data was most effective for tool wear classification.

by unrelated signal when compared to an acoustic sensor, as it is closer to the mining interface and collects signal from a more narrow bandwidth.

Table 5.4 Confusion Matrix for Tool Wear Classifier; Normalized by prediction
All Materials, All Penetrations, 0.2s Window, 50:50 test and train, Normalized Time Domain Data

% Pred.	Strain Gauge Prediction			Cap. Prediction		
	True Class	New	Mod.	Worn	New.	Mod.
New	0.983	0.105	0.000	1.000	0.000	0.000
Mod.	0.016	0.893	0.015	0.000	0.980	0.082
Worn	0.001	0.002	0.985	0.000	0.020	0.918

5.7 Conclusion

A sensor suitable for *in-situ* sensing of vibration signatures for material and wear classification was developed and tested for underground mining using conical picks. The classification accuracy achieved in the laboratory tests indicates that this is a promising technology for this application. The capacitive sensing design is low cost and low power due to its flexible circuit design. This technology could assist operators in material and wear classification by providing an objective measurement without requiring the operators to enter known hazardous regions near the machine and mining interface.

The capacitive load cell, to the authors knowledge, has not been used publicly for conical picks in rock cutting applications. This is a relatively new sensor technology that has been enabled by the steady advancement of capacitive sensor research over the last few decades. Existing solutions for hazard monitoring in underground coal mining primarily identify problems after they begin. Existing research in improving operator performance and safety has included acoustic classification systems and algorithms, strain-gauge based solutions, and piezo-electric sensors. By shifting the paradigm to predictive maintenance and more responsive control, operators are enabled to be safer and more efficient.

5.8 Disclosures

5.8.1 Conflicts of interests

On behalf of all authors, the corresponding author states that there is no conflict of interest. This work was funded by NIOSH Contract 75D30119C05413, “IMPROVING HEALTH AND SAFETY OF MINING OPERATIONS THROUGH DEVELOPMENT OF THE SMART BIT CONCEPT FOR AUTOMATION OF MECHANICAL ROCK EXCAVATION UNITS AND DUST MITIGATION”.

CHAPTER 6

YOUR JOURNAL PAPER TITLE GOES HERE

Modified from a paper to be published in The Journal of ABC¹.

Jane Jones^{2,3}, Sam Smith⁴, Ann Adams^{2,5}

6.1 Abstract

This is the abstract that is part of the paper. At the bottom of this page, beneath a 1.5" to 2" footnote line, can be footnotes with details of permission granted by the publisher of the paper, the author's titles and institution names, the relative contributions of each of the authors, et. If the abstract does not completely fill the page, the introduction also starts on this page. There are no page breaks between the different sections within the paper.

6.2 Introduction

The text of the introduction starts on the same page as the abstract, as long as there is room for at least two lines of text beneath the heading (This L^AT_EX template should look for this automatically.) The headings within this chapter will match the style used in the rest of the thesis. All pages of text within the paper are completely filled in.

6.3 Permissions

Make sure you have checked the journal permissions about reproducing your paper in your thesis. Make sure you put these permissions in the Appendix ??.

6.4 The next section of the paper

A lot more information from the paper that is being added into this dissertation. I would add figure, tables and other materials the same way as I have been in the other section of the dissertation. The big difference between this and the other chapters is the very top with the Journal and authors centered on the page.

Here is another paragraph that is just filler text. Lorem ipsum dolor sit amet, consectetuer adipiscing elit. Ut purus elit, vestibulum ut, placerat ac, adipiscing vitae, felis. Curabitur dictum gravida mauris.

¹Reprinted with permission of J. of ABC, 25(1), 41-45.

²Graduate student and Associate Professor, respectively, at the Colorado School of Mines

³Primary researcher and author

⁴Different Institution and position

⁵Author for correspondence

Nam arcu libero, nonummy eget, consectetuer id, vulputate a, magna. Donec vehicula augue eu neque. Pellentesque habitant morbi tristique senectus et netus et malesuada fames ac turpis egestas. Mauris ut leo. Cras viverra metus rhoncus sem. Nulla et lectus vestibulum urna fringilla ultrices. Phasellus eu tellus sit amet tortor gravida placerat. Integer sapien est, iaculis in, pretium quis, viverra ac, nunc. Praesent eget sem vel leo ultrices bibendum. Aenean faucibus. Morbi dolor nulla, malesuada eu, pulvinar at, mollis ac, nulla. Curabitur auctor semper nulla. Donec varius orci eget risus. Duis nibh mi, congue eu, accumsan eleifend, sagittis quis, diam. Duis eget orci sit amet orci dignissim rutrum.

CHAPTER 7

THIS IS THE TITLE OF A PAPER INCLUDED IN A THESIS

Reproduced with the permission for The Journal of ABC. 5[1]text

Jane Jones, Sam Smith, Ann Adams

7.1 Abstract

This is the abstract that is part of the paper. If the abstract does not completely fill the page, the introduction also starts on this page. There are no page breaks between the different sections within the paper.

7.2 Introduction

The text of the introduction starts on the same page as the abstract, as long as there is room for at least two lines of text beneath the heading (This L^AT_EX template should look for this automatically.) The headings within this chapter will match the style used in the rest of the thesis. All pages of text within the paper are completely filled in.

The next chapter shows another example with some foot notes for the authors, and the permission form the journal. Here is another quick sentence to make this paragraph look longer than it actually is, and not adding any new information for you to use.

CHAPTER 8

LOAD CELL DESIGN COMPARISON

Force on the cutting tool is determined by the tool geometry and the material. The force is also influenced by the dynamics of the machine. The physical sensor system also has dynamics, and depending on the model, these dynamics can be non-stationary. For rock cutting, two different capacitive load cell designs were tested.

The first design that was tested had non-linear, non-stationary dynamics.

The second design was more linear and the bias could be tracked and compensated.

The air gap design could work for applications with more gentle load profiles.

CHAPTER 9

LONGER DOWNSAMPLING RATES FOR ACOUSTIC CLASSIFICATION

The effect of increased sample length and downsampling

The effect of different frequency preprocessing methods

The effect of different window shapes

CHAPTER 10

ANALYTICAL MODEL FITTING

Dynamic system comparison between strain gauges and sensor

Plots of channel values and force prediction

Able to estimate side and drag forces as well, but normal force has greatest magnitude.

In the appendix we have MATLAB code for the sensor models, simulation procedure for calculation of capacitance and fringing effects, and the laser weld procedure used to assemble the sensor.

REFERENCES

- [1] Benjamin Hopkins Miller. Smartbit: in-situ bit/rock interface monitoring device, 2003. URL <http://hdl.handle.net/11124/170545>.
- [2] Sakir Selcuk. Analysis of coefficient of rock strength and measurement of percussive penetration rates and bit wear, 1981. URL <http://hdl.handle.net/11124/14359>.
- [3] Allen D. Gray. New types of drill rounds for development openings, 1952. URL <http://hdl.handle.net/11124/13192>.
- [4] Augustus L. Moore. Investigation of rock drill bits, an, 1946. URL <http://hdl.handle.net/11124/16423>.
- [5] Param Jit Singh. Study of the development of rock drill bits with special reference to the calumet and hecla copper company bits, a, 1948. URL <https://hdl.handle.net/11124/176345>.
- [6] C. Jobes, J. Carr, and J. Ducarme. Evaluation of an advanced proximity detection system for continuous mining machines. *International Journal of Applied Engineering Research*, 7(6):649–671, 2012.
- [7] J. Bartels, Christopher Jobes, Tim Lutz, and J. Ducarme. Evaluation of work positions used by continuous miner operators in underground coal mines. volume 53, 10 2009. doi: 10.1518/107118109X12524444080792.
- [8] Yaodong Jiang, Yixin Zhao, Hongwei Wang, and Jie Zhu. A review of mechanism and prevention technologies of coal bumps in china. *Journal of rock mechanics and geotechnical engineering (Online)*, 9(1):180–194, 2017. ISSN 1674-7755.
- [9] Mine Safety and Health Administration (MSHA). Niosh mine and mine worker charts. Online, 10 2021. Available: <https://www.cdc.gov/NIOSH-Mining/MMWC>.
- [10] NIOSH. Hierarchy of controls, Jan 2015. URL <https://www.cdc.gov/niosh/topics/hierarchy/default.html>.
- [11] JR Bartels, CC Jobes, JP DuCarme, and TJ Lutz. Evaluation of work positions used by continuous miner operations in underground coal mines. In *Proceedings of the Human Factors and Ergonomics Society*, pages 1622–1626. Human Factors and Ergonomics Society, 2009.
- [12] J. Mitchell. Research into a sensor-based diagnostic maintenance expert system for the hydraulics of a continuous mining machine. In *Conference Record of the 1991 IEEE Industry Applications Society Annual Meeting*, pages 1192–1199 vol.2, 1991. doi: 10.1109/IAS.1991.178014.
- [13] P. T. Bissert, JL Carr, and JP Ducarme. Proximity detection zones: Designts to prevent fatalities around continuous mining machines. *Professional safety*, 61(6):72–77, 2016.
- [14] Laxman S Sundae. *Measurement of coal-cutting forces underground with the in-seam tester*, volume 9033. US Department of the Interior, Bureau of Mines, Wachington, DC, 1985.
- [15] Donna L. Anderson. Laser tracking and tram control of a continuous mining machine. *Report of investigations (United States. Bureau of Mines)*, 9319, 1990. URL <https://stacks.cdc.gov/view/cdc/10570>.

- [16] M. J. Pazuchanics and Gary L. Mowrey. Recent progress in discriminating between coal cutting and rock cutting with adaptive signal processing techniques. *Report of investigations (United States. Bureau of Mines)*, 9475, 1993. URL <https://stacks.cdc.gov/view/cdc/10218>.
- [17] David Myers. Predicting mining machine cutting tool wear using neural networks, 1999. URL <http://hdl.handle.net/10388/11756>.
- [18] Hou-Lun Warren Shen. *Acoustic emission potential for monitoring cutting and breakage characteristics of coal*. The Pennsylvania State University, 1996.
- [19] Benjamin Hopkins Miller. Smartbit: in-situ bit/rock interface monitoring device, 2003. URL <http://hdl.handle.net/11124/170545>.
- [20] Witold Biay, Jiri Fries, and Greg Galecki. Determination of coal cutting forces using the cutting head of pou-bw/01-wap device. *Multidisciplinary Aspects of Production Engineering*, 4(1):281–289, 2021. doi: doi:10.2478/mape-2021-0025. URL <https://doi.org/10.2478/mape-2021-0025>.
- [21] *Utilizing Linear Cutting Machine Test for Estimating Cutting Force via Intact Rock Properties*, volume All Days of U.S. Rock Mechanics/Geomechanics Symposium, 06 2021. ARMA-2021-1108.
- [22] Yutaka Sasaki et al. The truth of the f-measure. *Teach tutor mater*, 1(5):1–5, 2007.
- [23] David MW Powers. Evaluation: from precision, recall and f-measure to roc, informedness, markedness and correlation. *arXiv preprint arXiv:2010.16061*, 2020.
- [24] Robert Teale. The concept of specific energy in rock drilling. In *International journal of rock mechanics and mining sciences & geomechanics abstracts*, volume 2, pages 57–73. Elsevier, 1965.
- [25] Nikita Klyuchnikov, Alexey Zaytsev, Arseniy Gruzdev, Georgiy Ovchinnikov, Ksenia Antipova, Leyla Ismailova, Ekaterina Muravleva, Evgeny Burnaev, Artyom Semenikhin, Alexey Cherepanov, et al. Data-driven model for the identification of the rock type at a drilling bit. *Journal of Petroleum science and Engineering*, 178:506–516, 2019.
- [26] Miho Klaic, Zrinka Murat, Tomislav Staroveski, and Danko Brezak. Tool wear monitoring in rock drilling applications using vibration signals. *Wear*, 408:222–227, 2018.
- [27] Issam Abu-Mahfouz. Drilling wear detection and classification using vibration signals and artificial neural network. *International Journal of Machine Tools and Manufacture*, 43(7):707–720, 2003.
- [28] Xu Tao and Feng Zhigang. Tool wear identifying based on emd and svm with ae sensor. In *2009 9th International Conference on Electronic Measurement & Instruments*, pages 2–948. IEEE, 2009.
- [29] Xu Tao and Wang Tao. Cutting tool wear identification based on wavelet package and svm. In *2010 8th World Congress on Intelligent Control and Automation*, pages 5953–5957. IEEE, 2010.
- [30] Liping Liu, Feng Wu, Chunliang Qi, Tianshu Liu, and Jing Tian. High frequency vibration analysis in drilling of gfrp laminates using candlestick drills. *Composite Structures*, 184:742–758, 2018.
- [31] Peng Nie, Zhengqiang Li, Yanchun Liu, Xinyu Liu, and Hongyao Xu. Study on identification method of tool wear based on singular spectrum analysis and support vector machine. In *2011 Second International Conference on Digital Manufacturing & Automation*, pages 1164–1167. IEEE, 2011.
- [32] Yiqiu Qian, Jia Tian, Libing Liu, Yu Zhang, and Yingshu Chen. A tool wear predictive model based on svm. In *2010 Chinese control and decision conference*, pages 1213–1217. IEEE, 2010.

- [33] Manel Martínez Ramón, Thomas Atwood, Silvio Barbin, and Christos G Christodoulou. Signal classification with an svm-fft approach for feature extraction in cognitive radio. In *2009 SBMO/IEEE MTT-S International Microwave and Optoelectronics Conference (IMOC)*, pages 286–289. IEEE, 2009.
- [34] Chih-Chung Chang and Chih-Jen Lin. Libsvm: a library for support vector machines. *ACM transactions on intelligent systems and technology (TIST)*, 2(3):1–27, 2011.
- [35] John C. Platt. Probabilistic outputs for support vector machines and comparisons to regularized likelihood methods. In *ADVANCES IN LARGE MARGIN CLASSIFIERS*, pages 61–74. MIT Press, 1999.
- [36] Sayan Mukherjee, Edgar Osuna, and Federico Girosi. Nonlinear prediction of chaotic time series using support vector machines. In *Neural Networks for Signal Processing VII. Proceedings of the 1997 IEEE Signal Processing Society Workshop*, pages 511–520. IEEE, 1997.
- [37] Jie Sun, Geok Soon Hong, Mustafizur Rahman, and YS Wong. The application of nonstandard support vector machine in tool condition monitoring system. In *Proceedings. DELTA 2004. Second IEEE International Workshop on Electronic Design, Test and Applications*, pages 295–300. IEEE, 2004.
- [38] Hongzhi Hu, Chang Qin, Fang Guan, and Haitao Su. A tool wear monitoring method based on woa and knn for small-deep hole drilling. In *2021 International Symposium on Computer Technology and Information Science (ISCTIS)*, pages 284–287, 2021. doi: 10.1109/ISCTIS51085.2021.00065.
- [39] Jeng-Fung Chen, Shih-Kuei Lo, and Quang Hung Do. An approach to the classification of cutting vibration on machine tools. *Information*, 7(1), 2016. ISSN 2078-2489. doi: 10.3390/info7010007. URL <https://www.mdpi.com/2078-2489/7/1/7>.
- [40] Alex J Smola and Bernhard Schölkopf. A tutorial on support vector regression. *Statistics and computing*, 14(3):199–222, 2004.
- [41] Rui Kong and Bing Zhang. Autocorrelation kernel functions for support vector machines. In *Third International Conference on Natural Computation (ICNC 2007)*, volume 1, pages 512–516. IEEE, 2007.
- [42] Ajit Tamhane and Dunlop Dunlop. Statistics and data analysis: from elementary to intermediate. page 280, 2000.
- [43] Dong-Hyuk Lee, Uikyum Kim, Hosang Jung, and Hyouk Ryeol Choi. A capacitive-type novel six-axis force/torque sensor for robotic applications. *IEEE Sensors Journal*, 16(8):2290–2299, 2016. doi: 10.1109/JSEN.2015.2504267.
- [44] Andrea Bodini, Stefano Pandini, Emilio Sardini, and Mauro Serpelloni. Design and fabrication of a flexible capacitive coplanar force sensor for biomedical applications. In *2018 IEEE Sensors Applications Symposium (SAS)*, pages 1–5, 2018. doi: 10.1109/SAS.2018.8336775.
- [45] Hyung-Kew Lee, Jaehoon Chung, Sun-Il Chang, and Euisik Yoon. Normal and shear force measurement using a flexible polymer tactile sensor with embedded multiple capacitors. *Journal of Microelectromechanical Systems*, 17(4):934–942, 2008. doi: 10.1109/JMEMS.2008.921727.
- [46] Kaspar Willam. Constitutive models for engineering materials. *Encyclopedia of physical science and technology*, 3:603–633, 2002.

- [47] Gianluca Barile, Alfiero Leoni, and Giuseppe Fern. A differential capacitive multi-material 3d printed sensor for portable anemometric applications. In *2019 IEEE 8th International Workshop on Advances in Sensors and Interfaces (IWASI)*, pages 234–238, 2019. doi: 10.1109/IWASI.2019.8791283.
- [48] Yunfeng Lu, Yang Bai, Tao Zeng, Zhengkun Li, Zhonghua Zhang, and Jiubin Tan. Coplanar capacitive sensor for measuring horizontal displacement in joule balance. In *2016 Conference on Precision Electromagnetic Measurements (CPEM 2016)*, pages 1–2, 2016. doi: 10.1109/CPEM.2016.7540791.
- [49] Ievgen O. Zaitsev and Anatolii S. Levytskyi. Determination of response characteristic of capacitive coplanar air gap sensor. In *2017 IEEE Microwaves, Radar and Remote Sensing Symposium (MRRS)*, pages 85–88, 2017. doi: 10.1109/MRRS.2017.8075034.
- [50] Gaurav Prit, Prateek Goyal, and Tarikul Islam. A novel design of the parallel plate capacitive sensor for displacement measurement. In *2019 IEEE 16th India Council International Conference (INDICON)*, pages 1–4, 2019. doi: 10.1109/INDICON47234.2019.9029007.
- [51] Xiaokang Liu, Kai Peng, Ziran Chen, Hongji Pu, and Zhicheng Yu. A new capacitive displacement sensor with nanometer accuracy and long range. *IEEE Sensors Journal*, 16(8):2306–2316, 2016. doi: 10.1109/JSEN.2016.2521681.
- [52] Martijn Schouten, Remco Sanders, and Gijs Krijnen. 3d printed flexible capacitive force sensor with a simple micro-controller based readout. In *2017 IEEE SENSORS*, pages 1–3, 2017. doi: 10.1109/ICSENS.2017.8233949.
- [53] Gerjan Wolterink, Remco Sanders, and Gijs Krijnen. Thin, flexible, capacitive force sensors based on anisotropy in 3d-printed structures. In *2018 IEEE SENSORS*, pages 1–4, 2018. doi: 10.1109/ICSENS.2018.8589584.
- [54] Ryan van Dommelen, Julien Berger, Rubaiyet I. Haque, Marco R. Binelli, Gilberto de Freitas Siqueira, Andr R. Studart, and Danick Briand. Fully 3d printed mechanical pressure sensors: A comparison of sensing mechanisms. In *2020 IEEE SENSORS*, pages 1–4, 2020. doi: 10.1109/SENSORS47125.2020.9278862.
- [55] Milica Kisi, Nelu Bla, Ljiljana ivanov, and Mirjana Damnjanovi. Capacitive force sensor fabricated in additive technology. In *2019 42nd International Spring Seminar on Electronics Technology (ISSE)*, pages 1–5, 2019. doi: 10.1109/ISSE.2019.8810154.
- [56] Saleem Khan, Leandro Lorenzelli, and Ravinder S. Dahiya. Technologies for printing sensors and electronics over large flexible substrates: A review. *IEEE Sensors Journal*, 15(6):3164–3185, 2015. doi: 10.1109/JSEN.2014.2375203.
- [57] P.K. Valavalas, T.C. Clancy, G.M. Odegard, and T.S. Gates. Nonlinear multiscale modeling of polymer materials. *International Journal of Solids and Structures*, 44(3):1161–1179, 2007. ISSN 0020-7683. doi: <https://doi.org/10.1016/j.ijsolstr.2006.06.011>. URL <https://www.sciencedirect.com/science/article/pii/S0020768306002198>.
- [58] Buwaneth Y. Dharmadasa, Matthew McCallum, and Francisco Lopez Jimenez. *Characterizing and modeling the viscoplastic behavior of creases in Kapton polyimide films*. doi: 10.2514/6.2020-2165. URL <https://arc.aiaa.org/doi/abs/10.2514/6.2020-2165>.
- [59] Hongzhou Li, Jialian Chen, Qinghua Chen, and Ming Liu. Determining the constitutive behavior of nonlinear visco-elastic-plastic pmma thin films using nanoindentation and finite element simulation. *Materials & Design*, 197:109239, 2021.

- [60] Wei He, Philippe Goudeau, Eric Le Bourhis, Pierre-Olivier Renault, Jean Christophe Dupré, Pascal Doumalin, and Shibin Wang. Study on young's modulus of thin films on kapton by microtensile testing combined with dual dic system. *Surface and Coatings Technology*, 308:273–279, 2016.
- [61] Yuemin Wang, Lei Shang, Panpan Zhang, Xiangqiao Yan, Ke Zhang, Shuliang Dou, Jiupeng Zhao, and Yao Li. Measurement of viscoelastic properties for polymers by nanoindentation. *Polymer Testing*, 83:106353, 2020.
- [62] Wen-Yang Chang, Te-Hua Fang, and Yu-Cheng Lin. Physical characteristics of polyimide films for flexible sensors. *Applied Physics A*, 92(3):693–701, 2008.
- [63] Pal Jen Wei, Wei Xin Shen, and Jen Fin Lin. Analysis and modeling for time-dependent behavior of polymers exhibited in nanoindentation tests. *Journal of non-crystalline solids*, 354(33):3911–3918, 2008.
- [64] Yuchao Zhu, Yigen Wu, Guangshun Wang, Zhongbao Wang, Qiulin Tan, Libo Zhao, and Dezhi Wu. A flexible capacitive pressure sensor based on an electrospun polyimide nanofiber membrane. *Organic Electronics*, 84:105759, 2020. ISSN 1566-1199. doi: <https://doi.org/10.1016/j.orgel.2020.105759>. URL <https://www.sciencedirect.com/science/article/pii/S1566119920301452>.
- [65] Jagoda A Dobrzynska and Martin AM Gijs. Flexible polyimide-based force sensor. *Sensors and Actuators A: Physical*, 173(1):127–135, 2012.
- [66] Andrea Bodini, Stefano Pandini, Emilio Sardini, and Mauro Serpelloni. Design and fabrication of a flexible capacitive coplanar force sensor for biomedical applications. In *2018 IEEE Sensors Applications Symposium (SAS)*, pages 1–5, 2018. doi: 10.1109/SAS.2018.8336775.

SELECTED BIBLIOGRAPHY

Read a book!

APPENDIX

SPECIAL COOLNESS.

Here is an example of added MATLAB code for a .m file (located in supporting-files/). The code can be referenced (Listing A.1).

Listing A.1: A MATLAB “Hello World“ Example

```
% Below is the example code for the absolute most popular program EVER!
disp('Hello\_World');
```